Experimental aerodynamic investigation of a Krueger flap device using Particle Image Velocimetry

Geoffrey Tanguy, Jean Claude Monnier*, Christophe Verbeke*, Jochen Wild***

**Univ. Lille, CNRS, ONERA, Arts et Metiers Paris Tech, Centrale Lille, Laboratory of Fluid Mechanics of Lille Kampé de Fériet F-59000, France*

Geoffrey.tanguy@onera.fr

***DLR – German Aerospace Center, Braunschweig, Germany*

Abstract

This paper presents the initial assessment of one of the validation experiments of the Unsteady High-lift Aerodynamics – Unsteady RANS validation project (UHURA). The aim of the study is to investigate the unknown aerodynamic characteristics of a slotted Krueger flap during deployment and retraction phases. The DLR-F15 airfoil model was equipped with a full span actuated Krueger device. A test campaign was conducted at the ONERA L1 wind tunnel. The test included measurements of steady and unsteady pressures along with phase locked Particle Image Velocimetry to achieve high quality validation data for the UHURA project. The results highlighted the transient behaviour of the flow during the deployment of the Krueger.

1. Introduction

The Unsteady High-lift Aerodynamics – Unsteady RANS Validation project (UHURA) investigates experimentally and numerically [1], [2] the aerodynamics of a Krueger flap leading edge device. The Krueger is an additional lift surface that is deployed from the lower side of the wing for take-off and landing [3]. The concept of the Krueger was initiated in 1940s [4] as a promising slotless high-lift system. Later it was implemented on the early Boeing passenger jets B707, B727, B737, and B747 "Jumbo". The slotted variant was identified as a suitable leading edge system for laminar wing technology during the NASA B757 laminar wing flight test program [5]. However, due to its complexity and the potential development of critical unsteadiness within the flow during the deployment, classical slat devices providing higher aerodynamic performance were preferred by aircraft manufacturers [6] and were highly investigated in the literature [7], [8].

In the future, aircraft designs may require laminar wings to meet the emission reduction targets set by ACARE FlightPath 2050 for future air transportation. The integration of high lift system for laminar wings remains one of the main challenges in the field as classical high-lift configurations using slat devices are proscribed with laminar wings due to the introduction of turbulence into the flow over the upper side of the wings. In addition, there is a need to shield the leading edge of the wings during low altitude flights, where pollution and insects could adversely impact the laminarity of the main wings for cruise conditions [6]. The slotted Krueger device's capability to shield the leading edge of the wing during take-off and landing along with its promising performances make it a suitable candidate for laminar wing devices.

Building on the learnings from the EC funded project DESIREH [3], [9], [10], the objective of the UHURA project is to investigate the unknown aerodynamic characteristics of the slotted Krueger device during deployment and retraction (Figure 1). This 3-phase project aims to validate unsteady flow simulation methods to determine the aerodynamic properties of the Krueger device during its motion. The first phase of the project defined the appropriate flow problem by designing the Krueger device. The second phase focused on unsteady flow simulations methods using Computational Fluid Dynamics (CFD) and experimentation setting up a series of wind tunnel tests to obtain high-quality validation data. Wind tunnel tests are foreseen in three different wind tunnels with two models to cover a broad range of conditions including variation of Krueger span (full span – part span), wing sweep angle and Reynolds

number. The third phase of the project is dedicated to assessing and validating the simulation results using the experimental data.

A recent wind tunnel test campaign was conducted at ONERA Lille during Fall 2021 using the DLR-F15 [11] airfoil model with a full span Krueger device, which can be actuated at high deflection rates up to 300°/s. The tests include the measurements of steady and unsteady static pressures as well as phase-locked Particle Image Velocimetry (PIV) on the lower section of the wing. The test results will be used as a reference data base to validate state of the art unsteady CFD methods simulating the unsteady flowfield during the deployment and retraction phase of the Krueger [12], [13]. This paper presents the preliminary assessment of the experimental results obtained within the ONERA L1 campaign.

2. Experimental methodology

2.1. The ONERA L1 facility

The ONERA L1 wind tunnel is an Eiffel-type low speed tunnel encapsulated within a 27m long, 14m wide and 13m height building providing a return section (Figure 2). The wind tunnel can be operated with either a closed or an open test section. For the UHURA project, the bespoke dodecagonal test section has been used. The section has a diameter of 2.4m and can provide a wide optical access thanks to modular glass or opaque panels (Figure 3a). The flow is driven by a 3.80m diameter fan up to 75m/s within the closed test section corresponding to a Reynolds number based on the square root of the test section of 1.06×10^6. The DLR-F15 model is mounted vertically in the test section. The model is placed on a motorised rotating axis able to perform a variation of the angle of attack.

2.2. DLR-F15 wing model with an actuated Krueger

The model used in this study is the DLR-F15 wing model with an actuated Krueger. The wing has a reference chord of 0.6m and a span of 2.4m. The wing model has already been tested in the framework of a ONERA-DLR Common Research Project (LEAFCO) [14], which investigated the impact of flow control at the wing leading edge to improve the aerodynamic performance at high angle of attack. For the UHURA project, the wing leading edge was modified to receive an actuated Krueger device (Figure 1). The Krueger was designed with two main objectives [15]. The first one is to protect the upper surface flow of the wing from separation at high angle of attack (similar to a slat device) while the second one is to shield the wing nose from insect contamination, to avoid drag rise by an early transition of the boundary layer.

The leading-edge device mechanism was designed by project partner ASCO within the UHURA project (Figure 1). The Krueger is made of three parts including a bull noise, a Krueger flap and the kinematic stations. The Krueger extends over the full span of the wing using three flaps of 0.8m long and six kinematics stations. The deployment of the Krueger is controlled with a main shaft, which induces a rotation of the flap and the bull noise (Figure 1). A transition strip is placed at the leading edge of the wing in order to ensure the presence of a turbulent boundary layer and improve the future comparison with CFD solution based on Reynolds-averaged Navier-Stokes (RANS) simulations.

For the L1 experiment, the main shaft is linked via a 1:50 reduction gear to a 5.3 kW-controlled servomotor with a nominal rotation speed of 3000 RPM positioned on top of the working section. The angular acceleration of the Krueger can go up to 1000 $°.s^{-2}$, which can provide a maximum deployment and retraction time of 0.8 seconds. The engine is equipped with a drive measurement and control unit providing torque and the rotational speed of the shaft. In addition, an external angular sensor located at the end of the drive shaft is used in order to measure the position of the Krueger during the deployments. The Krueger dynamic is adjusted with a dedicated software, which can fully control the sequence of the deployments and retractions. The engine of the Krueger is mounted on top of the working section on a structure made of ITEM and LINOS struts, which permits a fine adjustment of the engine alignment with the main Krueger shaft (Figure 3a). The engine sequence can be triggered with an external TTL signal and programmed to execute cycles of deployment and retraction. Therefore, the wind tunnel, PIV system and Krueger engine can be synchronized during the measurements thanks to an external master clock and delay generators.

Two types of deployments are performed in order to characterize the aerodynamics of the Krueger. The first one, referred as “static deployments”, measures the flow field for fixed position of the Krueger. The Krueger angle is set using the control software and maintained during the acquisition. The second type is referred as “dynamic deployments,” where multiple cycles of deployment and retraction are performed during the measurements of the

transient flowfield. For this project, multiple configurations of cycles are investigated by varying the deployment and retraction time.

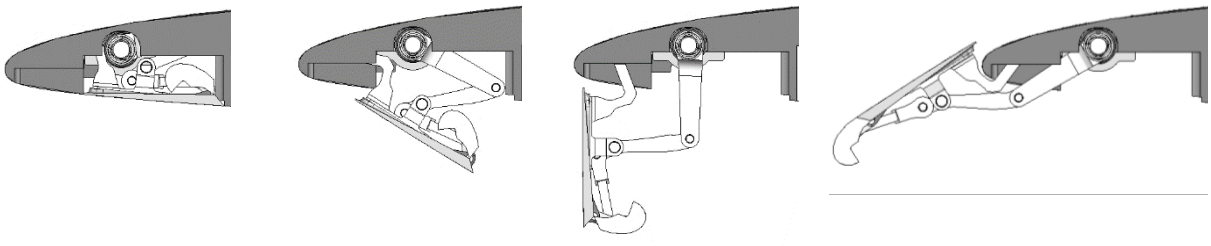

Figure 1 Deployment of the Krueger device

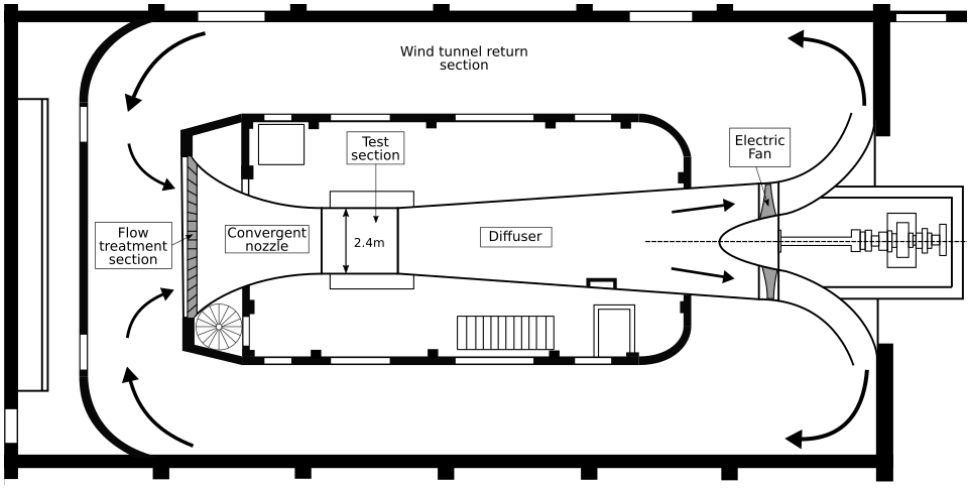

Figure 2 Illustration of the L1 wind tunnel (top view)

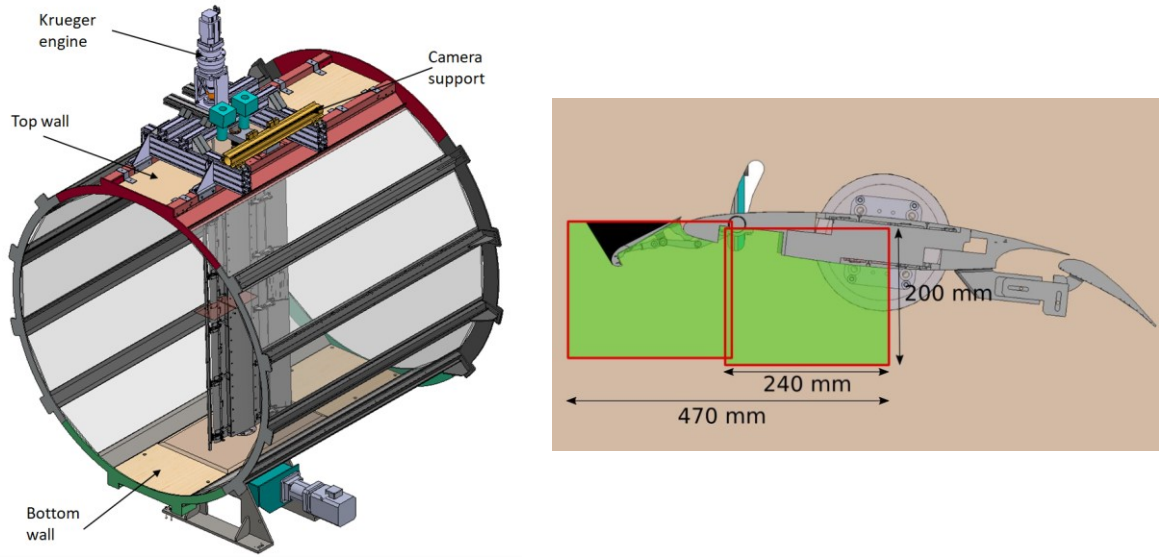

a) UHURA set up in the do-decagonal test section

b) CAD model and estimated PIV windows size and locations

Figure 3 Illustration of the UHURA wind tunnel set up at the ONERA L1

2.3. Pressure measurements

The DLR-F15 model is built with several static pressure ports with the majority located at the mid span of the wing. Several pressure taps are also spread across the wing near the side walls. These pressure taps are used to measure the wall static pressure in order to obtain the distribution of the pressure coefficient of the wing. In total, 139 taps are pneumatically connected with three MPS4263 pressure scanner. The pressure is acquired at a frequency of 500 Hz during 5s. The model is also equipped with five high sensitive pressure transducers (Kulites XCQ-093). The pressure sensors are located on the surface of the main wing over the extrados and intrados.

In addition, 26 Bosch BMP388 MEMS sensors are implemented on dedicated circuit boards on the new wing leading edge and the Krueger flap to provide the transient pressure during the deployment and retraction phases. The maximum frequency of acquisition with the MEMS is 100 Hz in order to measure the pressure fluctuations due to the deployment of the Krueger. The acquisition of the MEMS is synchronized with the wind tunnel using a TTL signal to start the acquisition.

2.4. PIV set up and measurement synchronization

The flowfield over the lower surface of the wing is measured with a 2D2C PIV acquisition system. The measurement plane is located at the mid-span section of the wing (Figure 3a). The two PIV windows measure the 2D2C velocity flow field over the lower surface of the wing from the leading edge of the Krueger to about half of the model chord (Figure 3b). The optical access for the PIV cameras is made possible by a bespoke upper endplate integrating a large glass window (Figure 4a). The size of the glass window used for optical access has been designed considering the field of view of the two SCMOS cameras and their characteristics. The estimated size of the PIV window based on the lens, focal and distance position of the camera was about 200mm by 240 mm. The two measurement planes overlap by about 15 mm. The measurement windows have been placed in order to capture the flow field during the full deployment of the Krueger. The largest flow separation that is expected when the Krueger is around 75° of deployment angle (almost vertical) was fully captured.

The velocity flow field is measured with two 5.5MP SCMOS cameras mounted on the top of the test section (Figure 4b). A dual cavity frequency-doubled pulsed Nd:YAG laser with a maximum power of 200mJ per pulse was used to illuminate the region of interest. The laser is mounted outside of the test section. A series of lenses and mirrors was used to deliver the laser beam into an estimated 2 mm thick light sheet to illuminate the lower surface mid-section plane of the wing (Figure 5a). The laser light is fired with a 40° angle from downstream in order to minimize the light obstruction during the Krueger deployment (Figure 5b). The PIV acquisition frequency for the UHURA test is at ONERA is 5Hz. For each test, a large number of PIV snapshots is acquired in order to perform the statistical analysis of the flow field.

Due to optical access, the cameras of the PIV system are slightly tilted by 3° to 4° from the plane orthogonal to the laser light sheet. This angle is corrected during the PIV process using a pinhole calibration procedure to dewarp the PIV images and to correct any misalignment between the plate and the laser sheet. A calibration target was made of a Cartesian grid with 20 mm spaced circular dots and placed in contact to the model using 3-points. The PIV images are processed with the in-house ONERA software FOLKI-SPIV [16] implemented on GPU providing a fast and accurate processing of the large amount of data acquired.

The PIV measurements are performed during the deployment and retraction of the Krueger. For “static deployments”, 2500 snapshots of the two PIV windows are acquired at a frequency of acquisition of 5Hz. Therefore, PIV measurements do not provide the detailed temporal component of the flowfield. However, the measurements enabled a statistical assessment of the flowfield. For the measurements of the “dynamics deployments,” which capture the transient flow downstream of the Krueger during the deployment and retraction phases, a phase locked averaging needs to be performed over multiple cycles in order to obtain averaged statistics of the flowfield. As a result, the synchronization between the PIV system and the Krueger kinematics needs to be perfect for each cycle. Each PIV snapshot requires to be acquired at the same Krueger angular position between cycles. A reasonably high number of cycle needs to be perform to obtain meaningful statistics of the flow field. In order to synchronize the measurement, each Krueger cycle (deployment + retraction) was triggered with a TTL signal synchronized with the PIV snapshots (Figure 6). This ensured to correct any delay within the Krueger deployment system.

a) b)

Figure 4 Photography of the model mounted in the test section (a) and PIV cameras set up (b)

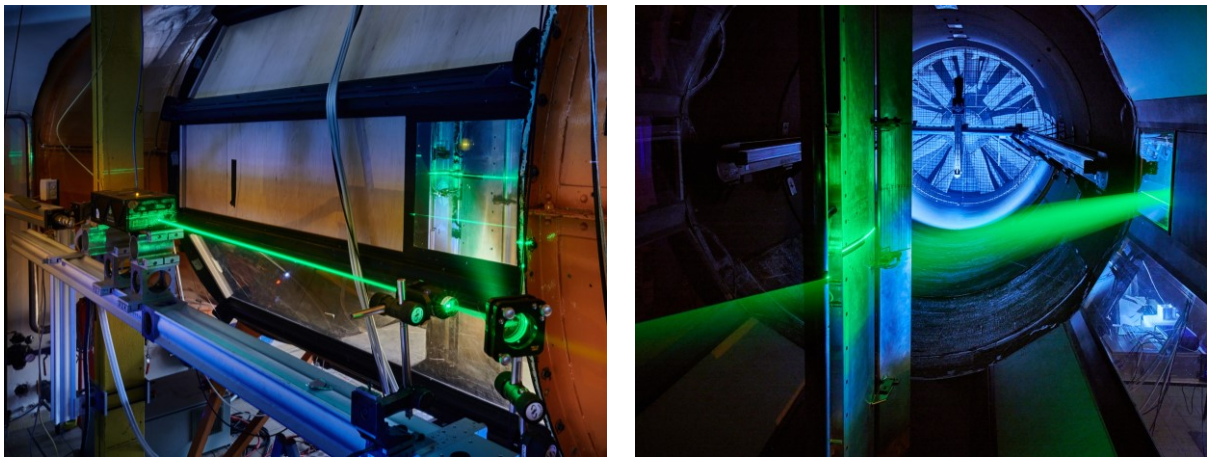

a) b)

Figure 5 Photography of the laser beam optical path (a) and sheet illuminating the model (b)

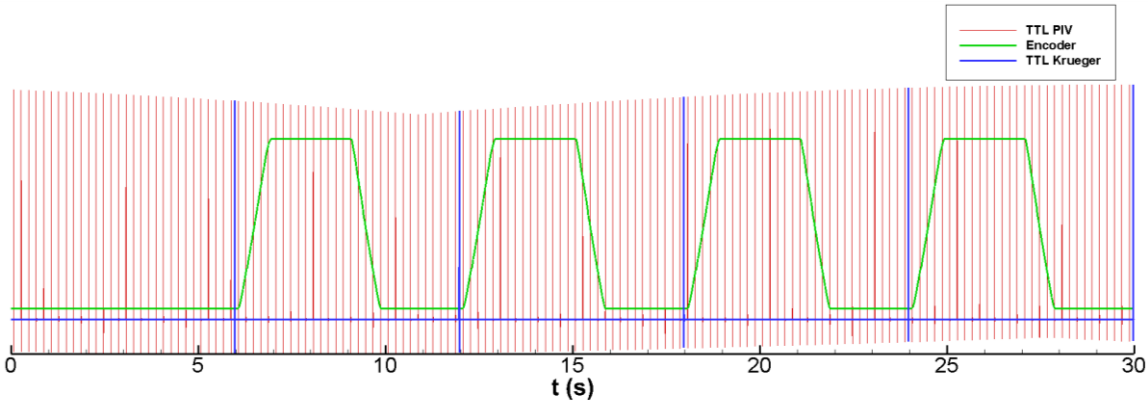

Figure 6 TTL and encoder signals measured by the tunnel acquisition during a dynamic deployment PIV test.

The frequency of acquisition of the PIV measurement is limited to 5 Hz and does not permit to resolve temporally the flow field. For a 1s deployment time (DT), the PIV system provides a snapshot every 28° of Krueger flap rotation. In order to increase the angular resolution of the deployment, the TTL used to start the Krueger cycles are delayed by 50, 100 and 150 ms providing an angular resolution of 7° equivalent to an acquisition frequency of 20 Hz.

2.5. Flow configuration

The DLR-F15 model is placed at an angle of attack (α) of 6° within the tunnel section and the rear flap angle of the wing is fixed at 30°. The effect of the free stream velocity is investigated with two U_{ref} equal to 30 and 45 m/s providing a chord based Reynolds number of respectively 1.15×10^6 and 1.73×10^6. The L1 wind tunnel operates at atmospheric pressure and temperature. The experimental campaign involved three types of test as listed below:

- Dynamic Krueger deployments and retractions cycles at $\alpha = 6°$.
- Static Krueger deployments at $\alpha = 6°$ for Krueger angles (δ_k) of 0°, 37.5°, 75°, 112.5° and 144.5°.
- Semi polar sweep from α = 0° to 30° with the Krueger closed ($\delta_k = 0°$) or fully deployed ($\delta_k = 144.5°$).

The total deployment time (DT) is also investigated during the experimental campaign for the dynamic tests. A DT of 4s, 2s and 1s was considered in order to investigate the possible dynamic amplifications of the wing aerodynamic characteristics due to the movement of the Krueger. As a result, the fastest deployment resulted in a maximum deflection speed of the Krueger $(\dot{\delta}_k)$ of about 200 °/s.

3. Results

3.1. Wing pressure distribution during a variation of incidence

The distribution of the static pressure coefficient for the wing at $\alpha = 6°$ and the retracted Krueger ($\delta_k = 0°$) shows a suction peak with high negative pressure levels up to $C_p = -9$ (Figure 7b). The stall of the wing at the leading edge occurs at an angle of attack between 8° and 10°. The pressure distribution around the flap of the wing also indicates a separated flow on the upper surface once the wing has stalled. A polar sweep from 0° to 30° was also performed with the Krueger fully deflected ($\delta_k = 144.5°$). The deployment of the Krueger significantly modifies the wall static pressure distribution of the main wing. Similar to a classical slat device, the main wing suction peak is reduced due to the lift generated by the Krueger device. The use of the Krueger flap considerably delays the stall of the wing. At $\alpha = 22°$, the rear wing and flap pressure distribution indicates a separated flow corresponding to the onset of the stall. The separation point then moves forward as the angle of attack increases and reaches the 20% of the chord at $\alpha = 26°$ (Figure 7i) associated with a reduction of the suction peak. The Krueger flap was designed to achieved a Cl_{max} around 22°, which is close to the stall angle from the wind tunnel campaign.

3.2. Static deployment flow investigation

Although one of the main objective of the UHURA project is to assess the flow field during the deployment of the Krueger device, several tests have been performed at fixed positions in order to provide reference data for RANS calculations. The measurement of static positions of the Krueger also gave the opportunity to check the convergence of the PIV flowfield statistics by using 2500 snapshots to calculate the mean and fluctuating velocity field. Fixed positions of the Krueger are also of interest as it reproduces scenarios where the Krueger is mal functioning.

The distribution of the static pressure coefficient for several Krueger angles (δ_k) is shown in Figure 8. For $\delta_k = 0°$, the static pressure coefficient associated with the bull nose indicate slightly higher pressures than on the lower surface of the main wing. This is associated to the pressure inside the cavity of the Krueger. As the Krueger is deployed, the stagnation point ($C_p = 1$) is moved from the leading edge to the Krueger flap until it reaches the bull nose. This is also visible from the velocity streamline from Figure 9 obtained from the PIV measurements. As soon as the Krueger start its deployment, the flow on the lower surface of the main wing separates. However, the PIV measurements indicate the presence of a flow jet passing through the gap between the main wing leading edge and the Krueger flap associated with high unsteadiness (Figure 9d).

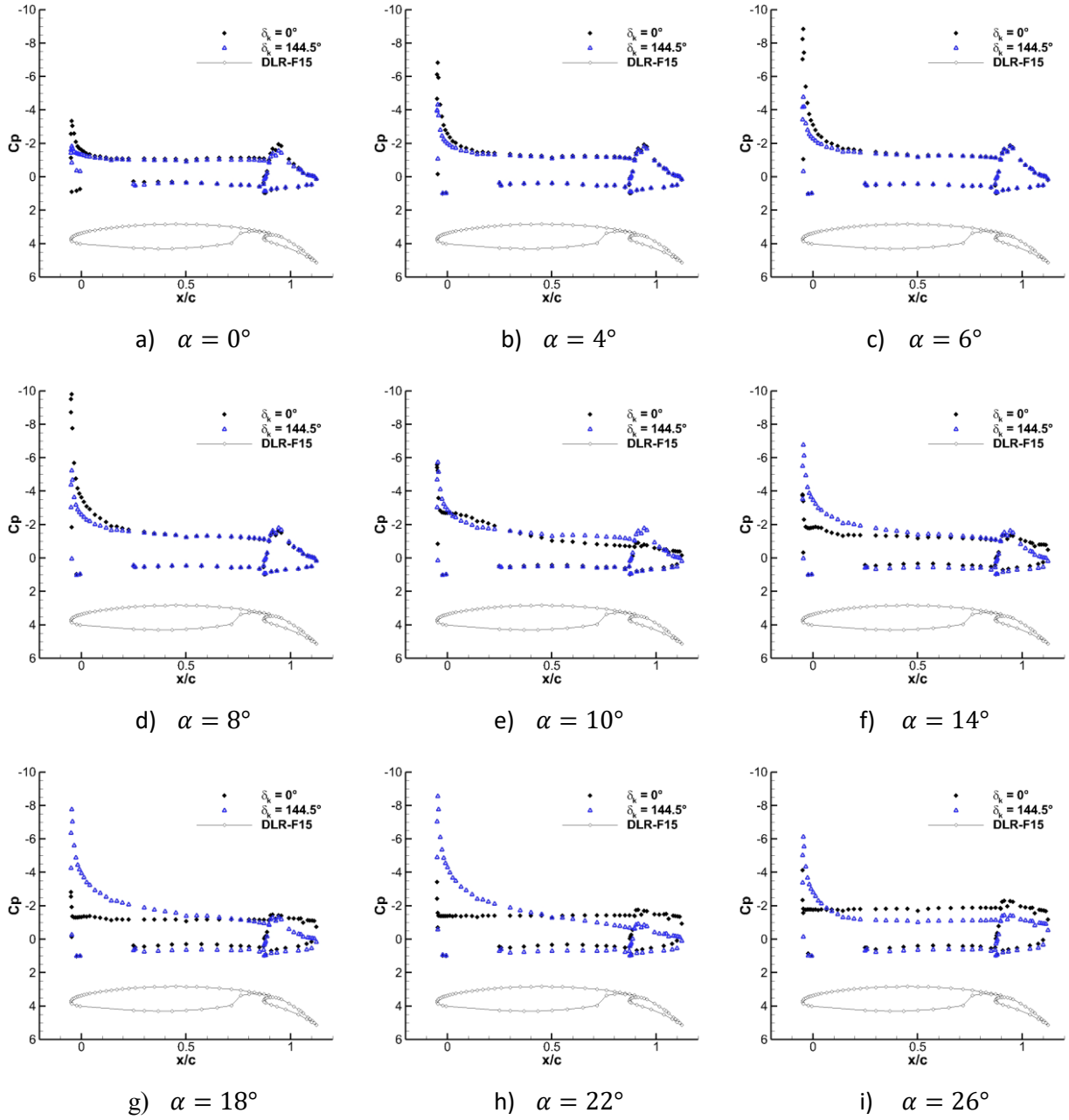

Figure 7 Static pressure coefficient distribution for the retracted ($\delta_k = 0°$) *and deployed* ($\delta_k = 144.5°$) *Krueger for* $U_{ref} = 45\ m/s$

When the Krueger angle is increased to 75°, the separation become critical with the presence of a shear layer. Downstream of the Krueger, the separated flow is made of two counter-rotating vortex structures (Figure 9e) associated with two distinct reverse flow regions (Figure 9f). The assessment of the Cp distribution for $\delta_k = 75°$ indicates a strong reduction of lift due to the lower ΔCp between the upper and lower surfaces (Figure 8c). Although the PIV setup measures only the velocity flow field on the lower surface up to the mid chord, the Cp distribution indicates that the flap of the wing becomes ineffective and that the flow on its upper surface is separated. Therefore, the Krueger angle $\delta_k = 75°$ seems to be the most critical phase during its deployment.

When the Krueger angle is further increased, the reattachment point of the lower surface flow is moved toward the leading edge of the wing. At $\delta_k = 112.5°$, the flow at the wing lower side reattaches slightly after the mid chord of the wing (Figure 9i) and the flap pressure distribution shows beginning reattachment of the flow at the flap, too

(Figure 8d). However, the thickness of the separated region remains high downstream of the Krueger flap. The structure of the flow is dominated with a counter-clockwise 2D vortex associated with high levels of unsteadiness.

Finally, when the Krueger is fully deployed, the lower surface flow is attached excepted for the region directly behind the bull nose (Figure 9k). The Cp distribution indicates the presence of distinct suction peaks on each element as commonly observed for high lift devices. The minimum Cp level for the Krueger flap is around -1.8 , while for the main wing leading edge, $Cp_{min} = -5$.

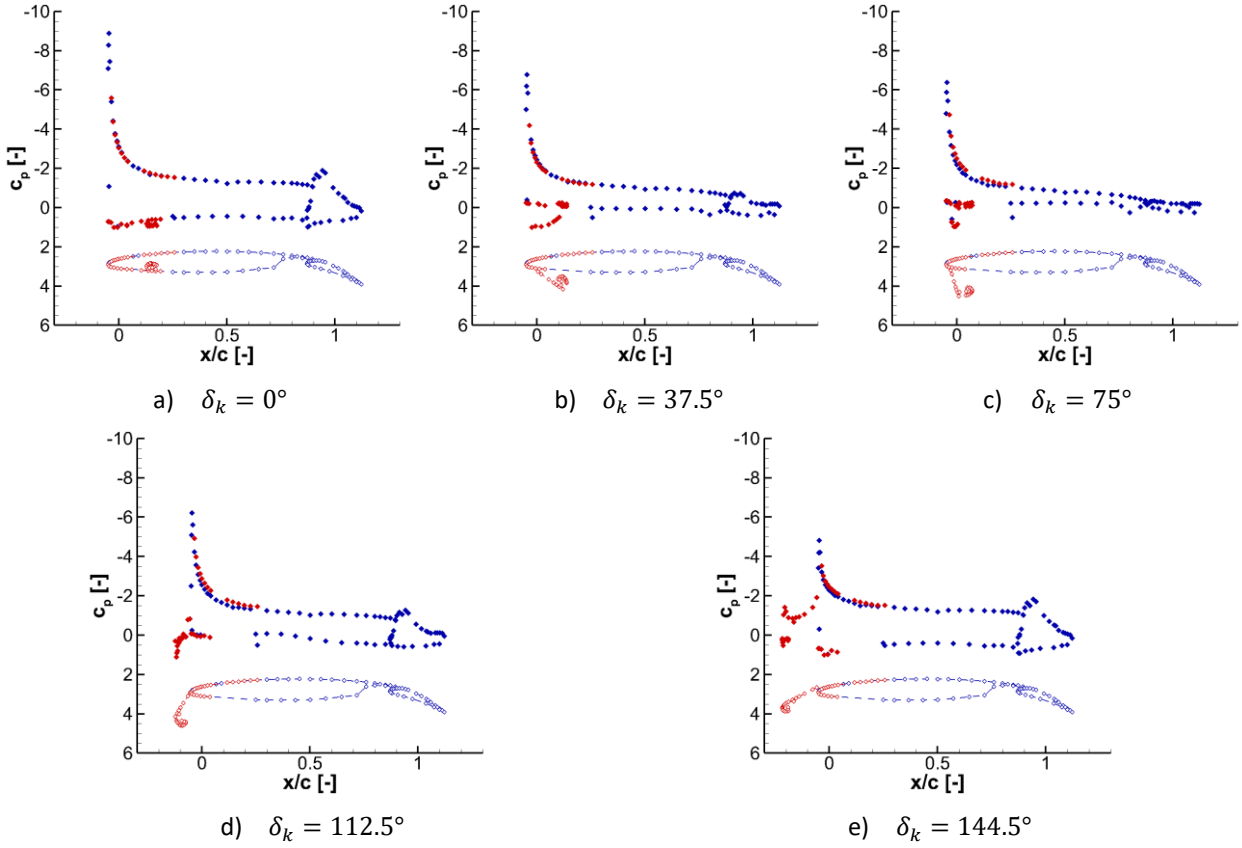

Figure 8 Static pressure coefficient distribution for several Krueger fixed positions at $\alpha = 6°$ and $U_{ref} = 45\ m/s$.

<u>*Convergence assessment for dynamic deployments*</u>

The UHURA project is dedicated to the validation of Unsteady Reynolds-averaged Navier-Stokes (URANS) calculation. In order to compare the PIV flowfield with an unsteady RANS solution, the time-averaged flowfield is computed from multiple PIV snapshots acquired at the same Krueger phase angle. Therefore, the PIV measurements are acquired during multiple cycles and sorted per phases. As a result, the time averaged and fluctuating velocity fields can be obtained for each phases. For static deployments, the time averaged and fluctuating flowfield at Krueger fixed positions was calculated over 2500 PIV snapshots. However, this is not possible for the dynamic deployments, as it would require performing 2500 deployment and retraction cycles for a single configuration. Figure 10 shows the averaged velocity magnitude and turbulent kinetic energy calculated for 50, 250, 500 and 2500 PIV snapshots for a static configuration where $\delta_k = 75°$. The computation of the averaged flowfield is rapidly converged relative to 2500 snapshots. However, for the calculation of the fluctuating velocity, even the use of 500 snapshots does not provide a fully converged solution. However, from the analysis of the turbulent kinetic energy profile located at x/c = 0.3 from the leading edge, the peak in k_{uv} due to the presence of the shear layer is overestimated by 9% for 500 snapshot compared with 2500 snapshot. As a compromise and due to technical restrictions, the dynamic phase lock averaged was made over 300 cycles.

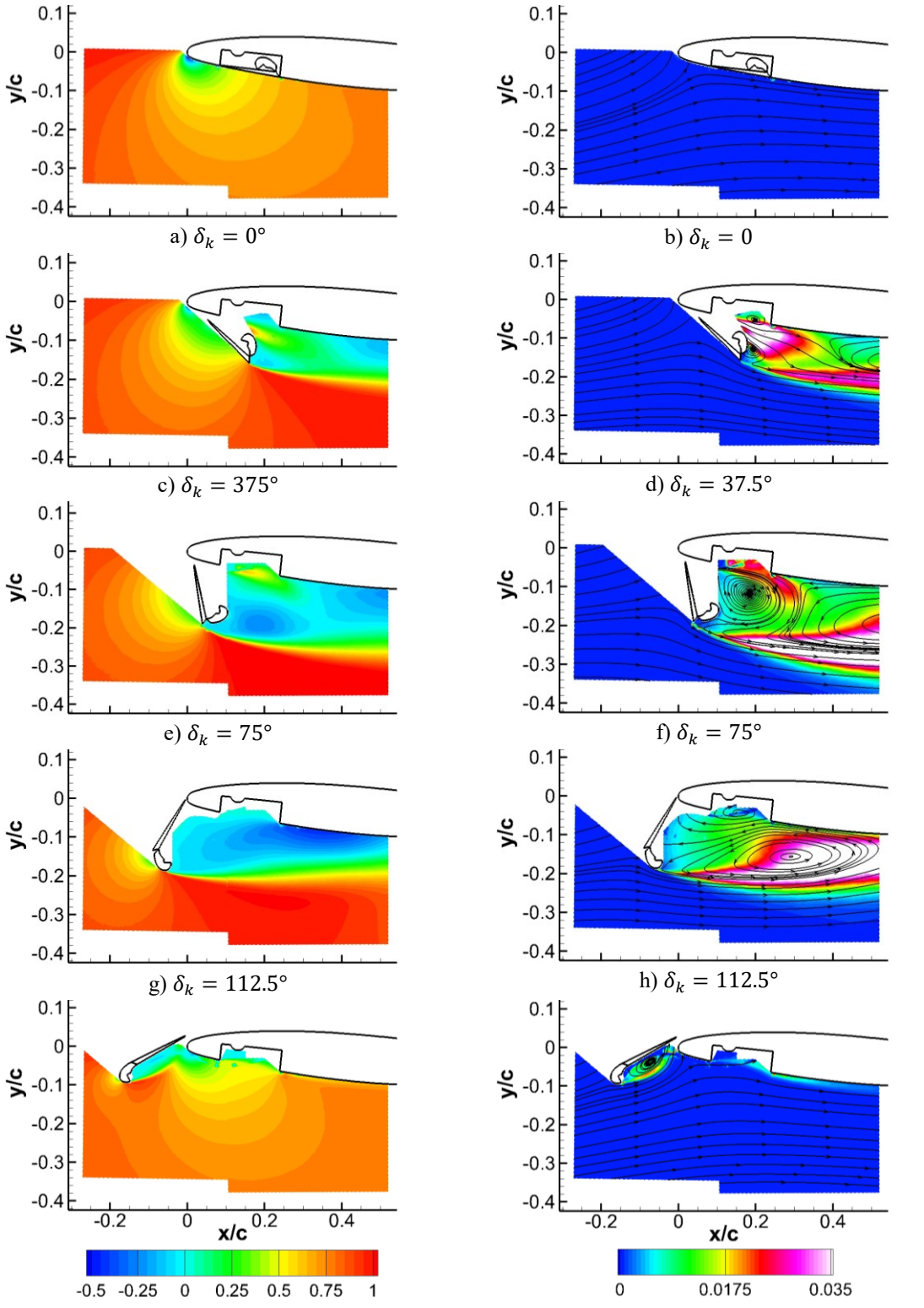

a) $\delta_k = 0°$ b) $\delta_k = 0$

c) $\delta_k = 375°$ d) $\delta_k = 37.5°$

e) $\delta_k = 75°$ f) $\delta_k = 75°$

g) $\delta_k = 112.5°$ h) $\delta_k = 112.5°$

i) $\delta_k = 144.5°$ j) $\delta_k = 144.5°$

Figure 9 Illustration of the time averaged longitudinal velocity $\frac{\langle U \rangle}{U_{ref}}$ and in-plane turbulent kinetic energy k_{uv}/U_{ref}^2 for several static position of the Krueger

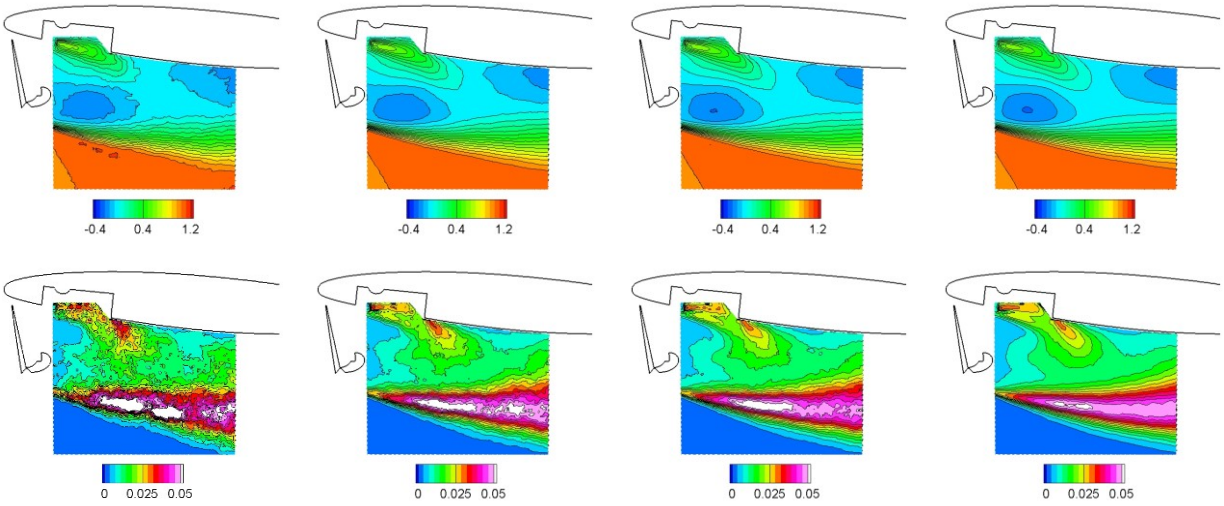

a) n = 50 b) n = 250 c) n = 500 d) n = 2500

Figure 10 Time averaged velocity ($\langle U \rangle / U_{ref}$) (Top row) and turbulent kinetic energy (k_{uv}/U_{ref}^2) (bottom row) calculated from n PIV snapshots for a Krueger fixed position ($\delta_k = 75°$) at $U_{ref} = 45\ m/s$

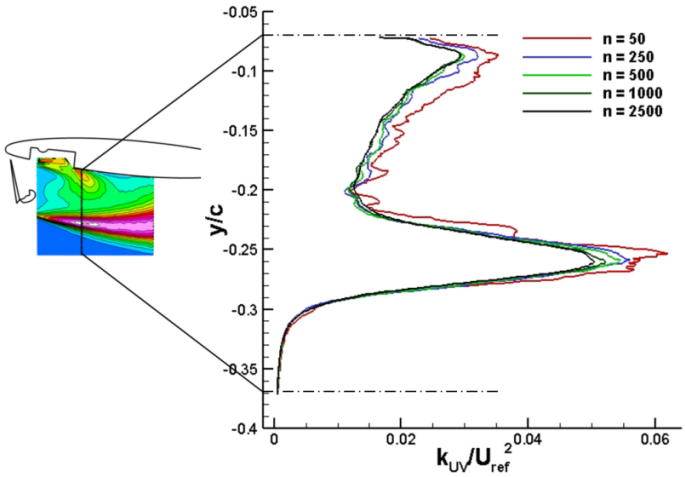

Figure 11 Turbulent kinetic energy profile at x/c = 0.3 calculated from n PIV snapshots for a Krueger fixed position ($\delta_k = 75°$) at $U_{ref} = 45\ m/s$

3.3. Dynamic deployment flow investigation

Instantaneous flowfield

The PIV flow field is measured during the deployment and retraction phase of the Krueger. The assessment of the instantaneous in-plane velocity magnitude calculated as $V_{mag} = (U^2 + V^2)^{0.5}$ and out-of-plane vorticity is provided in Figure 12. The deployment time (DT) used for this case is 4 seconds and the acquisition frequency of the PIV snapshots is 5Hz. As a result, the deployment is captured with 20 snapshots. One of the main difficulties associated with the measurement of moving parts, is the presence of laser light reflections and optical path obstructions, which depend on the Krueger position. Fortunately, the possible view obstruction due to the Krueger kinematic stations during the deployment was mitigated with the camera angle of view. However, it can be noted that some spurious vectors are calculated due to the presence of cables over the lower surface of the Krueger and at the leading edge of the wing (Figure 12i and k) originating from the dynamic MEMS sensors. Nevertheless, the quality of the measurements provides a detailed view of the instantaneous velocity and vorticity field during the Krueger deployment.

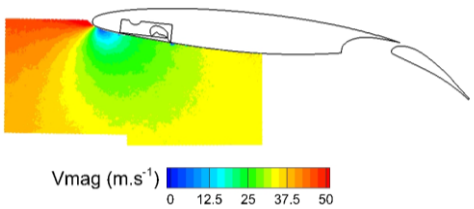

a) δ_k = 0°

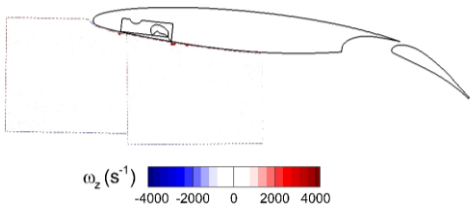

b) δ_k = 0°

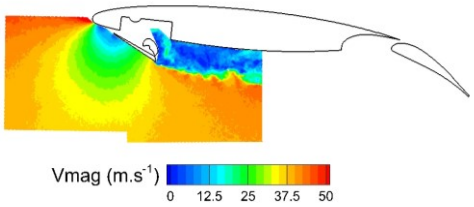

c) δ_k = 23.0°

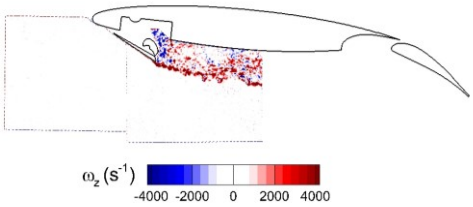

d) δ_k = 23.0°

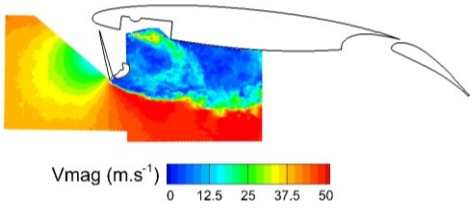

e) δ_k = 44.1°

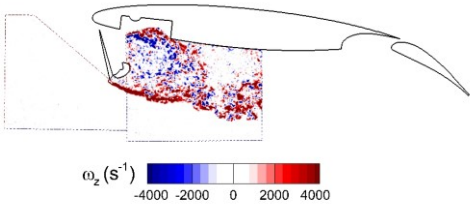

f) δ_k = 44.1°

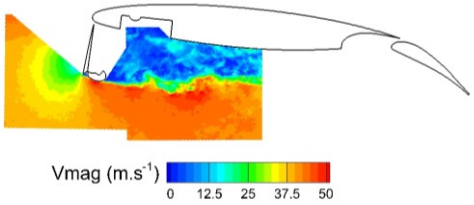

g) δ_k = 82.4°

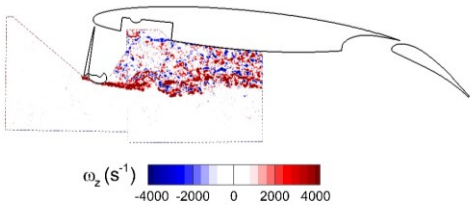

h) δ_k = 82.4°

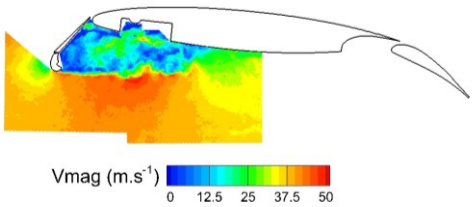

i) δ_k = 116.2°

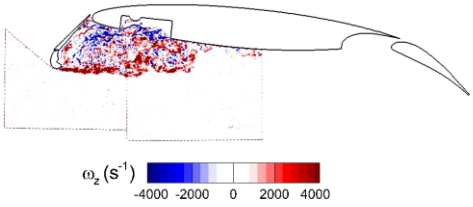

j) δ_k = 116.2°

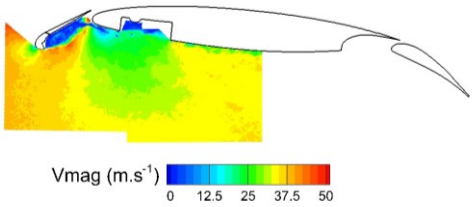

k) δ_k = 144.5°

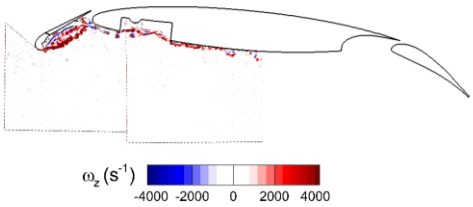

l) δ_k = 144.5°

Figure 12 Instantaneous velocity magnitude (left) and out-of-plane vorticity (right) during the Krueger deployment from PIV measurements for $U_{ref} = 45\ m/s$

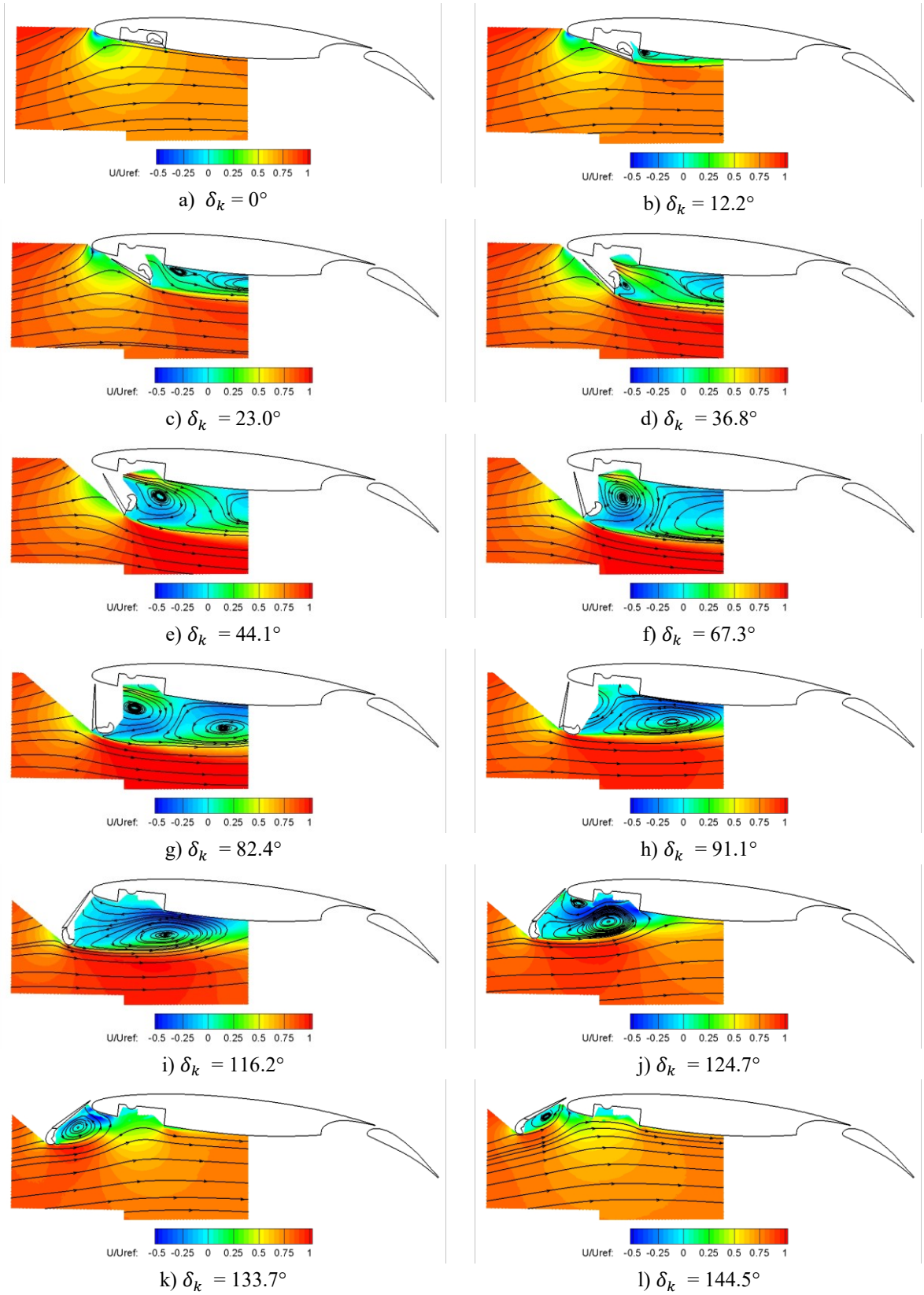

a) $\delta_k = 0°$ b) $\delta_k = 12.2°$

c) $\delta_k = 23.0°$ d) $\delta_k = 36.8°$

e) $\delta_k = 44.1°$ f) $\delta_k = 67.3°$

g) $\delta_k = 82.4°$ h) $\delta_k = 91.1°$

i) $\delta_k = 116.2°$ j) $\delta_k = 124.7°$

k) $\delta_k = 133.7°$ l) $\delta_k = 144.5°$

Figure 13 Phase averaged longitudinal velocity U/Uref during the Krueger deployment (DT = 4s) from PIV measurements for $U_{ref} = 45\ m/s$

The out-of-plane vorticity (Figure 12) field shows that the Krueger produces a shear layer associated with both large detached and small-scale eddy structures. When the Krueger is fully deployed, the perturbation of the flow due to the Krueger is confined on its lower surface as expected. However, the boundary layer on the pressure side of the main wing is contaminated with turbulent structures rising from the flow within the Krueger cavity, which could affect the aerodynamic of the wing. The results also demonstrate that a partial or an uncompleted deployment of the Krueger will significantly affect the flow under the main wing with potentially a decrease of the lift and a significant increase of the drag. Therefore, the Krueger high-lift device needs to be fully deployed to provide an acceptable flowfield for flight conditions. Overall, the PIV measurements provide a sufficient quality to assess the instantaneous flowfield over the lower surface of the wing. Further analysis will be performed in order to identify how each position of the device influences the main flow modes.

Phase locked averaged flowfield

The analysis of the phase locked average flowfield for DT = 4s (slow deployment) is presented in Figure 13. The synchronisation between the Krueger engine and the PIV system (Figure 6) was a success. The fact that each Krueger cycle (deployment and retraction) was triggered with the PIV signal permitted to remove any large internal jitter that could appear over long test runs. The analysis of the encoder signal demonstrated that overall, during deployment or retraction, the uncertainty of the Krueger angles due to mechanical or electrical jitter during the test were equal to $\sigma_{\delta_k} = \pm 0.5°$. As a result, the phase averaged longitudinal velocity flowfield for selected phases is computed in Figure 13.

The in-plane velocity streamlines shows the complex evolution of the flow structure as the Krueger is deployed. When the Krueger starts its movement, a separation bubble associated with an anticlockwise rotating vortex appears aft the cavity of the wing at x/c = 0.24 with a reattachment of the flow around x/c = 0.45 (Figure 13b). For a Krueger angle of 23°, the length of the separation increases with the presence of a second rotating cell. Unfortunately, half of this second vortex is out of the PIV window (Figure 13c). However, the lower wing boundary layer seems to be fully separated until it reaches the rear flap. When the Krueger angle is at $\delta_k = 36°$, the incoming freestream flow that goes through the gap between the Krueger flap and the wing leading edge forms a high velocity jet-like flow, which suppresses the first separation bubble identified previously. However, the Krueger flap creates a new separation region around the bull nose associated with a clockwise vortex (Figure 13d). When the Krueger angle is further increased to $\delta_k = 82.4°$ (Figure 13g), the bull nose separation becomes dominant supplied with the flowfield coming from the gap between the Krueger and the wing. As a result, two distinct swirling regions are formed behind the Krueger. At this position, the Krueger is perpendicular to the freestream flow and it should represent one of the worst position for the aerodynamics performances of the wing. Passed $\delta_k = 82.4°$, the increase of δ_k tends to reduce the size of the bull nose separation region and the anticlockwise vortex becomes dominant within the separated flow. As the Krueger angle is further increased to $\delta_k = 116.2°$ (Figure 13i), the size of the separation region is decreased and the flow is reattached around x/c = 0.51. Interestingly, when $\delta_k = 124.7°$, the reverse flow near the cavity forms a separation bubble associated with a clockwise vortex (Figure 13j). When the Krueger reaches its maximum angle, the flow separates just after the bull nose as expected and reattaches on the lower surface of the Krueger flap at about 90% of its length (Figure 13l). Therefore, the initial assessment of the flow during the deployment of the Krueger demonstrates various topologies associated the separation of the lower surface of the wing. The complexity of the flow and the quality the measurements provide a valuable validation case for the URANS computations that are performed within the UHURA project.

The averaged velocity profile at x/c = 0.5 (right hand side of the PIV windows) is extracted for each phase (Figure 14) in order to assess the velocity wake behind the Krueger during its deployment. The maximum size of the wake is achieved when the Krueger is perpendicular to the flow and can reach a thickness up to 25% of the chord, which is approximately double the size of the Krueger panel itself. In order to provide an initial assessment of the impact of Krueger deployment time (DT) over the flowfield, the mean velocity in the wake of the Krueger is computed from the extracted profiles at x/c = 0.5 for DT = 4s and 1s (Figure 15). The variation of the mean velocity in the wake of the Krueger $(\langle \bar{U} \rangle / U_{ref})_{wake}$ during the deployment and retraction phases is similar for DT = 4s (Figure 15a). However, it can be noted that the angles δ_k at which the PIV snapshots are acquired differs slightly from the deployment and retraction phase. For the measurements with a deployment time DT of 1s, there is a significant difference between $(\langle \bar{U} \rangle / U_{ref})_{wake}$ during the deployment and retraction phases (Figure 15b). The losses in the wake of the Krueger are increased when DT varies from 4s to 1s during the deployment, while for the retraction phase, the distributions of $(\langle \bar{U} \rangle / U_{ref})_{wake}$ are very similar. Therefore, this initial assessment demonstrates that the velocity loss associated with the separation of the flow on the lower surface of the wing increases with rapid deployments of the Krueger.

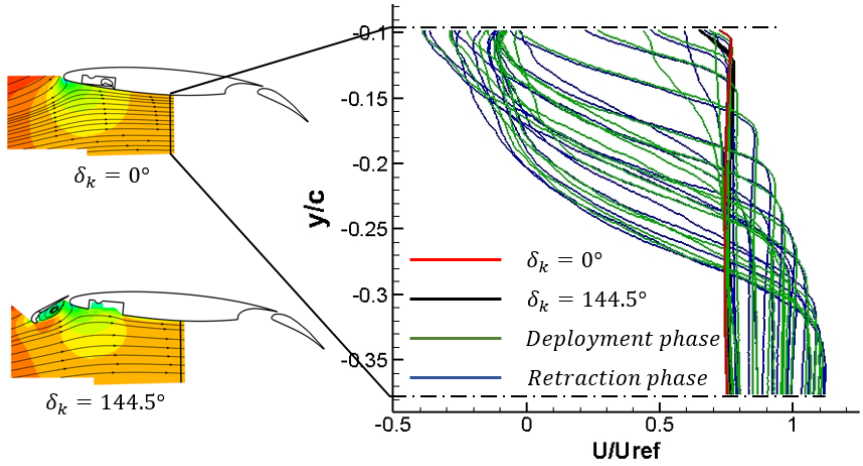

Figure 14 Time averaged velocity profile at x/c = 0.5 during the deployment and retraction of the Krueger for $DT = 4s$ *and* $U_{ref} = 45m/s$

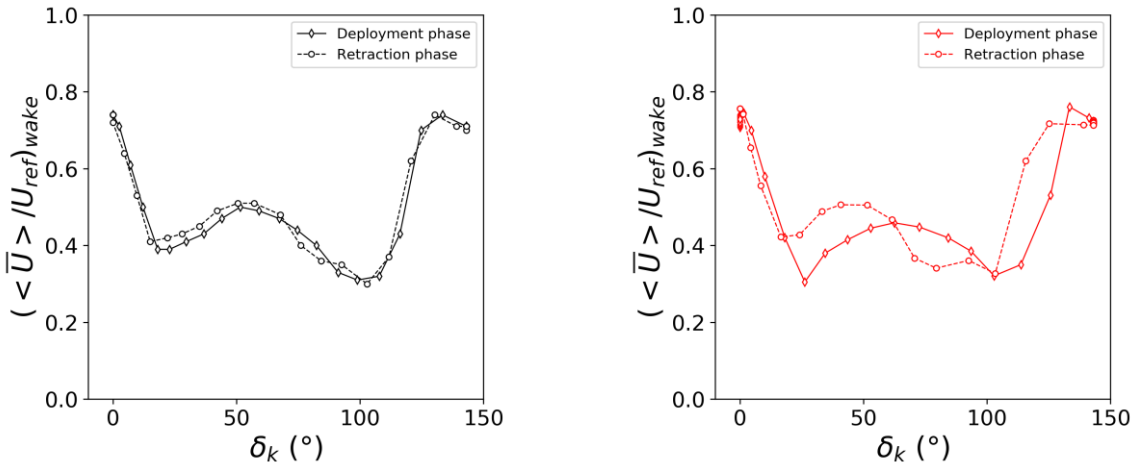

a) $DT = 4s$ b) $DT = 1s$

Figure 15 Mean velocity in the wake of the Krueger at x/c = 0.5 as a function of the Krueger flap angle (δ_k) *for deployment times of* (DT) *4s and 1s at* $U_{ref} = 45m/s$

4. Conclusion

This paper presents the initial assessment of the flowfield during the deployment of a Krueger device integrated to the DLR-F15 wing measured at the ONERA L1 wind tunnel. The synchronous acquisition of PIV measurements with the Krueger motion and static pressures permitted to assess the unsteady and phase lock averaged velocity flowfield developed over the lower side the wing. The in-plane velocity measurements highlighted the transient flow topology that constantly changes during the Krueger movement. The use of integrated MEMS pressure sensors captured the variation of static pressure on the Krueger surface during the deployment. The large database measured during the experimental campaign, which includes the effect of Krueger velocity deployment and wind tunnel velocity over the flowfield will serve as reference data to validate URANS calculations within the UHURA project.

5. Acknowledgments

The project UHURA has received funding from the European Union's Horizon 2020 research and innovation program under grant agreement No 769088.

References

[1] J. Wild, 'Unsteady High-Lift Aerodynamics – Unsteady RANS Validation; An Overview on the UHURA Project', in *10th EASN International Conference*, 2020.

[2] J. Wild, M. Schmidt, A. Vervliet, and G. Tanguy, 'A 2D Validation Experiment for Dynamic High-Lift System Aerodynamics', in *WCCM-ECCOMAS Congress*, 2020.

[3] H. Strüber and J. Wild, 'Aerodynamic design of a high-lift system compatible with a natural laminar flow wing within the desireh project', in *29th Congress of the International Council of the Aeronautical Sciences, ICAS*, 2014.

[4] W. Krueger, 'Systematic wind-tunnel measurements on a laminar wing with nose flap', *NACA TM 1119*, 1948.

[5] P. K. C. Rudolph, 'High-Lift Systems on Commercial Subsonic Airliners', *NASA Contractor Report 4746*, 1996.

[6] R. D. Joslin, 'Overview of Laminar Flow Control', *NASA Technical Paper*, 1998.

[7] C. L. Rumsey and J. P. Slotnick, 'Overview and summary of the second AIAA high-lift prediction workshop', in *Journal of Aircraft*, 2015, doi: 10.2514/1.C032864.

[8] T. Imamura, S. Enomoto, Y. Yokokawa, and K. Yamamoto, 'Three-dimensional unsteady flow computations around a conventional slat of high-lift devices', in *AIAA Journal*, 2008, doi: 10.2514/1.25660.

[9] J. Wild, 'Overview on the DeSiReH Project', *5th European Conference for Aerospace Sciences (EUCASS)*, 2013.

[10] S. Bosnyakov, E. Kazhan, I. Kursakov, S. Matyash, S. Mikhaylov, and A. Lysenkov, 'Aerodynamic performance of the DeSiReH high-lift laminar wing at free flight and ETW in-tunnel conditions', 2015, doi: 10.1051/eucass/201507033.

[11] J. Wild, 'Mach and reynolds number dependencies of the stall behavior of high-lift wing-sections', in *Journal of Aircraft*, 2013, doi: 10.2514/1.C032138.

[12] J. Ponsin and C. Lozano, 'Progress towards simulation of Krueger device motion with Lattice Boltzmann Methods', in *IOP Conference Series: Materials Science and Engineering*, 2021, doi: 10.1088/1757-899X/1024/1/012050.

[13] F. Capizzano and T. Sucipto, 'A dynamic Immersed Boundary method for moving bodies and FSI applications', in *IOP Conference Series: Materials Science and Engineering*, 2021, doi: 10.1088/1757-899X/1024/1/012049.

[14] V. Ciobaca and J. Wild, 'An Overview of Recent DLR Contributions on Active Flow-Separation Control Studies for High-Lift Configurations', *AerospaceLab*, 2013.

[15] I. Emiliano, Q. Domenico, and W. Jochen, 'Krueger High-Lift System Design Optimization', in *8th European Congress on Computational Methods in Applied Sciences and Engineering, ECCOMAS Congress*, 2022.

[16] F. Champagnat, A. Plyer, G. Le Besnerais, B. Leclaire, S. Davoust, and Y. Le Sant, 'Fast and accurate PIV computation using highly parallel iterative correlation maximization', in *Experiments in Fluids*, 2011, doi: 10.1007/s00348-011-1054-x.